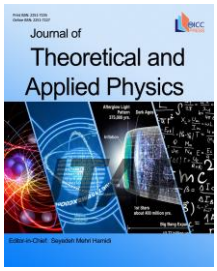

Volume 19, Issue 6, 192553 (1-10)

Journal of Theoretical and Applied Physics (JTAP)

https://doi.org/10.57647/j.jtap.2025.1906.53

Investigating the Impact of the Nuclear Single-Particle Potentials on Parity-Changing Transitions and Deformation in ^{24}Mg

Ali A. Alzubadi*, Ali K. Abood

Department of Physics, College of science, University of Baghdad, Baghdad, Iraq

***Corresponding author:** ali.abdullatif@sc.uobaghdad.edu.iq

Original Research

Received:
02 September 2024

Revised:
16 September 2024

Accepted:
13 August 2025

Published online:
31 December 2025

Abstract

The present work focuses on the nuclear structure of ^{24}Mg J^{π} (0^{+}), with particular emphasis on the low-lying positive and negative parity excited states and their associated electromagnetic form factors. The study utilizes a combination of the Shell Model (SM) and Skyrme Hartree-Fock (SHF) method, considering inelastic electroexcitation form factors for excitation energies up to 13 MeV in a momentum transfer range from 0.0 to 3.0 fm^{-1}. Various single-particle potentials, including SHF, HO, and WS models, are applied to describe positive and negative parity states. Additionally, the HF+BCS method is employed to investigate the quadrupole deformation (β_2) as a function of energy, offering insights into the shape and structure of nuclei. The results demonstrate a reasonable agreement between theoretical predictions and experimental data, particularly in reproducing longitudinal and transverse electroaxcitation form factors and energy level schemes. Notably, the HO potential exhibits better alignment with experimental data for specific transitions, indicating its effectiveness in capturing crucial features of nuclear structure. This study underscores the importance of one-body potentials, two-body effective interactions, and parameterization in accurately describing various nuclear systems, particularly those featuring unstable nuclei. The findings shed light on the behavior of ^{24}Mg, paving the way for further advancements in nuclear theory through the integration of theoretical frameworks.

Keywords: Nuclear shell model; Electroexcitation form factor; Different parity sates; Skyrme-Hartree-Fock; Quadrupole deformation

1. Introduction

The nuclear shell model (SM), hailed as the foremost theoretical framework, is essential in unravelling the inner structure of nuclei through nucleon interactions [1]. Its immense value lies in its precision in revealing nuclei's structural makeup, which has been extensively relied upon for this purpose. This influential model follows the principle of nucleons functioning independently within a central potential well, inspiring other major microscopic models [2]. The SM leading microscopic approach in the study of nuclear systems utilizes a diagonalized Hamiltonian to depict the system comprehensively. The SM has significantly influenced various macroscopic models by using a set of numerical values denoting two-body matrix (TBM) and single-particle energies (SPE). In order to combine these models, a diagonalized Hamiltonian featuring numerical representations of two-body matrix elements (TBME) and SPEs is commonly employed. The SM goes beyond the mean field (MF) by incorporating configuration mixing (CM) for a specific model space and number of particles [3]. In a mean field (MF) picture, nuclei are described as independent particles interacting only through the average MF potential created by the other nucleons [4]. This suggests that a widespread single-particle phenomenological model can replace the MF. However, this substitution requires a thorough computation of CM, encompassing all possible many-body states created from a range of single nucleon states

centered around the Fermi energy [5]. We must delve into the foundations of what has come before us to move forward. Reviewing the literature, we are amazed by some papers that paved the way for our current work. Alzubadi and Obaid [6] investigated the nuclear deformation of even–even isotopes of Ne, Mg, Si, S, Ar, and Kr using the Hartree-Fock-Bogoliubov (HFB) method and SLy4 Skyrme parameterization. Zarek et al. [7] conducted measurements on the electromagnetic form factors of ^{24}Mg, focusing on stronger transitions to negative parity states using electron energies ranging from 90 to 280 MeV and scattering angles of 90^{o} and 160^{o}. They compared their findings with open-shell random-phase approximation (RPA) calculations. Hotta et al. [8] performed measurements on transverse electron scattering form factors for iso-scalar transitions T=0 levels in ^{24}Mg at various energies, along with an unresolved T=0 doublet. Manie et al. [9] delved into the nuclear structure of the ^{24}Mg nucleus, employing self-consistent Hartree-Fock (HF) calculations within the framework of the SM.

Their study encompassed the computation of elastic and inelastic electron scattering form factors and transition probabilities for both positive and negative low-lying states.

Ogata [10], through microscopic structure analyses and reaction calculations, explored the negative-parity states of ^{24}Mg using proton and α inelastic scattering to enhance our understanding of the band assignment for the observed negative-parity spectra. Lees et al. [11], [12] conducted a study on the low-lying excited states in ^{26}Mg below 11 MeV excitation energy using inelastic electroexcitation with a momentum transfer range of 0.4 to 1.05 fm^{-1}. Additionally, they explored the excited states in ^{25}Mg within the momentum transfer range of 0.3 to 1.15 fm^{-1}.

The current study aims to investigate the transitions to different parity states in ^{24}Mg in order to gain a more comprehensive understanding of the underlying nuclear structure and dynamics.

This exploration also provides insights into symmetry-breaking phenomena within the nucleus, which are essential for elucidating the fundamental interactions governing nuclear structure. Two distinct SM spaces have been utilized for this investigation.

The first one is the sd-SM space for positive parity states, which includes the (1d5/2, 1d3/2, and 2s1/2) valence orbits. The renormalized G matrix for the sd-shell was initially developed in the mid-1960s by Kuo and Brown [13]–[15].

These G matrix interactions demonstrate reasonable agreement with the renormalized mid-sd-shell G matrix. Experimental spectra for A = 18 and A = 38 show fair consistency with these G matrix interactions. The present work introduces results for the updated USD-type Hamiltonians known as USDC, alongside the application of the USDA and USDE Hamiltonians.

The second shell model space is a truncated large-scale SM space spsdpf for negative parity states, which includes the 1s1/2, 1p3/2, 1p1/2, 2s1/2, 1d5/2, 1d3/2, 2p3/2, 2p1/2, 1f7/2 and 1f5/2 valence orbits are appropriately truncated for nuclei. Calculations within this SM space for this model space are conducted using the WBP Hamiltonian [16]. As previously stated, our main aim is to assess the electroexcitation form factors of parity change transitions in a ^{24}Mg nucleus. This involves demonstrating the influence of alterations in the nuclear single-particle potentials, energy levels and changes in the quadrupole deformation. We plan to calculate the radial wavefunctions of single-particle matrix elements for all excited states using the harmonic oscillator (HO), Wood Saxon (WS), and Skyrme Hartree-Fock (SHF) potentials.

2. Theoretical Consideration

2.1. Equations

The reduced matrix elements of the electroexcitation operator $\hat{O}^{\lambda}$ for an n-particle shell model space wavefunction of multipolarity λ are expressed as the sum of the product of the one-body transition density (OBTD) matrix elements and the reduced single-particle matrix elements. This can be given by the following equations [17]:

$$\begin{aligned}&\langle f \left\| \hat{O}^{\lambda} \right\| i\rangle = \\ &\langle n\omega_f J_f \| \hat{O}^{\lambda} \| n\omega_i J_i\rangle = \\ &\sum_{k_\alpha k_\beta} OBTD\,(fik_\alpha k_\beta \lambda)\langle k_\alpha \| \hat{O}^{\lambda} \| k_\beta\rangle\end{aligned} \tag{1}$$

where k stands for (nl_j) the single-particle states, i and f labels are a shorthand notation for the initial and final SM space states, ($n\omega_i J_i$) and ($n\omega_f J_f$), respectively. The ω indices distinguish between the various basis states with the same J value.

The OBTD in proton–neutron formalism is given by the following equation [17]:

$$OBTD\left(fik_{\alpha,t_z}k_{\beta,t_z}\lambda\right) = \frac{\langle n\omega_f J_f \| \left[a^{+}_{k_{\alpha,t_z}} \otimes \tilde{a}_{k_{\beta,t_z}}\right]^{\lambda} \| n\omega_i J_i\rangle}{\sqrt{2\lambda+1}} \tag{2}$$

For the central potential, we employ the Skyrme potential, which is a two-body interaction. The codes we use demonstrate that a one-body potential in HF theory can be derived from it. This potential is in the mean-field (MF) category, signifying that it is a one-body potential. Its purpose is to mimic the mean field resulting from all the nucleons constituting the nucleus, and to approximate the realistic nuclear-nuclear (NN) forces. The Skyrme effective interaction, leading to the Skyrme energy (E_{Skyrme}), is a two-body density-dependent interaction.

It models the strong force in the particle-hole channel and encompasses central spin-orbit and tensor

contributions in the coordinate space representation [18].

$$V_{Skyrme}(\vec{r}_1,\vec{r}_2) =$$

$$t_0(1+x_0\hat{p}_\sigma)\delta_{12} =$$

$$\frac{t_1}{2}(1+x_1\hat{p}_\sigma)[\vec{k}'^2\delta_{12}+\vec{k}^2\delta_{12}]$$

$$+t_2(1+x_2\hat{p}_\sigma)k'\delta_{12}k$$

$$+\frac{t_3}{6}(1+x_3\hat{p}_\sigma)p^\alpha(\frac{\vec{r}_1-\vec{r}_2}{2})\delta_{12}$$

$$+iW_0\vec{k}'\delta_{12}(\hat{\vec{\sigma}_1}+\hat{\vec{\sigma}_2})$$

$$\times\vec{k}+\frac{t_e}{2}([3(\hat{\vec{\sigma}_1}.\vec{k}')(\hat{\vec{\sigma}_2}.\vec{k}') \quad (3)$$

$$-(\hat{\vec{\sigma}_1}.\hat{\vec{\sigma}_2})\vec{k}'^2]$$

$$+\delta_{12}[3(\hat{\vec{\sigma}_1}.\vec{k})(\hat{\vec{\sigma}_2}.\vec{k})$$

$$-(\hat{\vec{\sigma}_1}.\hat{\vec{\sigma}_2})\vec{k}^2])$$

$$+t_0[3(\hat{\vec{\sigma}_1}.\vec{k})\delta_{12}(\hat{\vec{\sigma}_2}.\vec{k}')$$

$$-(\hat{\vec{\sigma}_1}.\hat{\vec{\sigma}_2})\vec{k}'\delta_{12}\vec{k}']$$

where $\delta_{12}=\delta(r_1-r_2)$ and k, k' are the relative momentum operators with k acting on the right, and k' on the left and are given by:

$$\hat{K}=\frac{1}{2i}(\vec{\nabla}_1-\vec{\nabla}_2),\hat{K}'=-\frac{1}{2i}(\vec{\nabla}_1'-\vec{\nabla}_2') \quad (4)$$

The spin-exchange operator denoted by $\hat{P}_\sigma$:

$$\hat{p}_\sigma=\frac{1}{2}(1+\hat{\sigma}_1.\hat{\sigma}_2) \quad (5)$$

In the Eq. (5), $\hat{\sigma}$ represents the Pauli spin matrices.
The Skyrme parameterizations denoted by xn, tn, to, te, α and Wo are the free parameters that define the strengths of the various interaction terms.
It is crucial to calibrate these parameters using experimental data on nuclear structure.
Each term generates both time-even and time-odd densities in the HF equations. The Coulomb (Longitudinal) electron scattering form factors are denoted by F(Cλ, q, f, i) for inelastic scattering between initial (i) and final (f) states, or for elastic scattering (i = f). The transverse electric and transverse magnetic form factors are denoted F(Eλ, q, f, i) and F(Mλ, q, f, i) respectively, where λ represents the multipolarity.
The last two types of form factors can be further broken down into components based on the convection currents λc (resulting from the orbital motion of the nucleons) and the magnetization currents λm (arising from the intrinsic magnetic moments of the nucleons) [19].

$$F(E\lambda,q,f,i) = F(E\lambda c,q,f,i)+F(E\lambda m,q,f,i) \quad (6)$$

$$F(M\lambda,q,f,i) = F(M\lambda c,q,f,i)+F(M\lambda m,q,f,i) \quad (7)$$

Hence, the overall longitudinal electron scattering form factor can be expressed as:

$$|F_C(q,f,i)|^2=\sum_{\lambda\geq 0}|F(C\lambda,q,i,f)|^2 \quad (8)$$

the total transverse electron scattering form factor is represented as:

$$|F_T(q,f,i)|^2 = \sum_{\lambda>0}\{|F(E\lambda,q,i,f)|^2+|F(M\lambda,q,i,f|^2\} \quad (9)$$

The electron scattering form factor, which involves the angular momentum J and the momentum transfer q between the initial and final nuclear SM states of spin Ji,f, can be expressed as follows [18]:

$$|F(X,\lambda,q,f,i)|^2 = N_P\left|\sum_{t_z}\langle n\omega_f J_f\|\hat{O}^\lambda(X_5,q,t_z)\|n\omega_i J_i\rangle\right|^2 \quad (10)$$

$$\times F_{cm}^2(q)F_{fs}^2(q)$$

The expression NP represents the equation $4\pi/Z^2(2J_i+1)$, where the character X is used to select the longitudinal (L or C) and transverse (T) form factors. These two nuclear form factors encompass all the details of nuclear physics. $F_{cm}(q)$ is the correction for the lack of translational invariance in the SM (center-of-mass correction), and $F_{fs}(q)$ is the nucleon finite size (fs) form factor. The total form factor is the combined result of the longitudinal and transverse terms.

$$|F(q)|^2=|F_C(q,f,i,)|^2 +[1/2+\tan^2(\theta/2)]|F_T(q,f,i)|^2 \quad (11)$$

where θ is the electron scattering angle.

The reduced transition probability is given by [17]:

$$B(X\lambda)=\frac{Z^2}{4\pi}\frac{[(2\lambda+1)!!]^2}{\omega^{2\lambda}}|F(X\lambda,k)|^2 \quad (12)$$

where $k=E_x/\hbar c$.B(M1) is in units of u_N^2, B(E2) is in units of "e^2fm^4, B(M2)" is units of $u_N^2fm^2$ and B(E1) is units of e^2fm^2, where u_N is the nuclear magneton.

$$u_N = \frac{e\hbar}{2m_p c} = 0.1051 \ e\,fm \qquad (13)$$

3. Results and Discussion

In the present study, the OBTD matrix elements are determined using the last updating NUSHELLX@MSU SM code [20], which consists of wrapper codes developed by Alex Brown. These wrapper codes utilize data files for model spaces and Hamiltonians to generate input for the code. NUSHELLX, a suite of computer codes developed by Bill Rae [21], is used to calculate precise energies, eigenvectors, and spectroscopic overlaps for low-lying states in SM Hamiltonian matrix calculations with large basis dimensions. It employs a J-coupled proton-neutron basis and can handle J scheme matrix dimensions of up to 100 million. The wrapper codes also transform the NUSHELLX output into figures and tables for energy levels, gamma decay, and beta decay. Subsequently, the OBTD elements are used to compute the matrix elements of Cλ, Eλ, and Mλ operators. The variation of quadrupole deformation parameter with energy is calculated using HF+BCS code, taking into account the collective motion of nucleons.

3.1. Positive Parity States

The longitudinal and transverse electroexcitation form factors from the ground-state to the isoscalar transitions in the ^{24}Mg nucleus have been evaluated for low-lying excited states in MeV; $2^+_{(1)}$ (1.368), $2^+_{(2)}$ (4.238), $3^+_{(1)}$ (5.235), $4^+_{(1)}$ (4.122) and $4^+_{(2)}$ (6.010). The inelastic C2 form factor for the transition to the first excited 2^+ state is specifically highlighted in Fig. 1(a). The results obtained using various nuclear single-particle potentials demonstrate reasonable agreement with experimental data. The positioning of the predicted first maximum at q=0.8 fm-1 and the second maximum at q≈ 2.0 fm^{-1} aligns well with the experimental maxima. While the position of the first maximum remains relatively stable and aligns well with the experimental data, the second maximum is slightly overpredicted in the theoretical calculations. This discrepancy suggests that there may be underlying factors or interactions not fully accounted for in the model, leading to an overestimation of the form factor at higher momentum transfers. We find that the first maximum's position scarcely changes, which is considerably more in line with the data and to second max is slightly over predicted, we notice compatibility at SLy4. The observed enhancement of the form factor in the first maximum is in accord with our findings, there is also a shift in the location of the second maximum, to larger values of q, however. The first diffraction minimum and the ratio of the second to the first maximum for the 2^+ transition is quite well matched by the calculations. The inelastic longitudinal C2 form factor for the transition to the second excited 2^+ state at 4.238 MeV is shown in Fig.1(b). It is clear that all the potentials accurately predict the strength and shape of the first maximum, although the peak is slightly shifted upward compared to the experimental data. To illustrate the effects of nuclear models on their ability to match experimental data and reproduce the overall trend, Fig. 1(c) shows the current C2 calculation for the second excited 2^+ state at 4.238 MeV using various models, including valence (VM), core polarization (CP), and Tassie (TM) models. It is evident that the Tassie model provides the best fit to the experimental data for this transition.

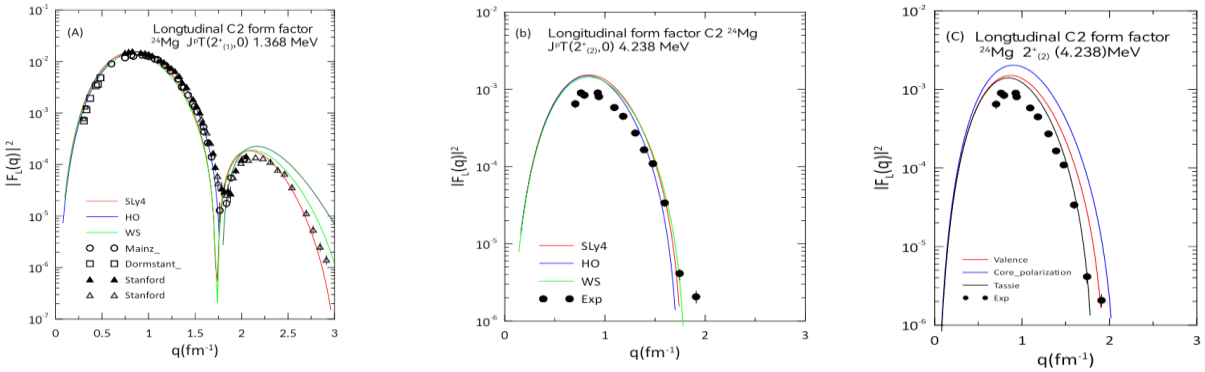

Figure 1. The first and second 2^+ (1.37, 4.238) MeV states' theoretical longitudinal form factors (a), (b) with various single potential and (c) different models compared to experiment results [8].

The transverse form factors are crucial for understanding the patterns of nuclear current. In the case of the ^{24}Mg isotope, which is a rotational nucleus with an even-even configuration, studying the inelastic transverse electroexcitation form factor from the ground state with angular momentum J helps us directly observe the electric EJ multipole of the nuclear current. This Fig. 2 (a) presents the USDC two-body effective interaction predictions for the transverse E2 form factor for the transition to low-lying excited states $2^+_{(1)}$ and $2^+_{(2)}$. The impact of adjusting the single-particle potential observation provides valuable insight into the current patterns related to collective motion within the nucleus. The transverse electroexcitation form factor associated with transitions to the excited states 2^+ and 4^+ states is purely electrical, while the form factor for the 3^+ transition is purely magnetic. The experimental data has been taken from Hotta et al. [8].

was examined and compared with experimental data. Upon careful examination, it was observed that the result obtained using the WS potential was superior to those obtained using other potentials. Furthermore, it was observed that the strength of the maximum is underestimated and that an effective charge is necessary to achieve better agreement with the experimental data. Fig. 2 (b) depicts the theoretical predictions for a $2^+_{(1)}$ transition. The agreement with the experimental data is good, where the strength of the predicted form factors is well predicted, and the location of the minimum is not correctly reproduced.

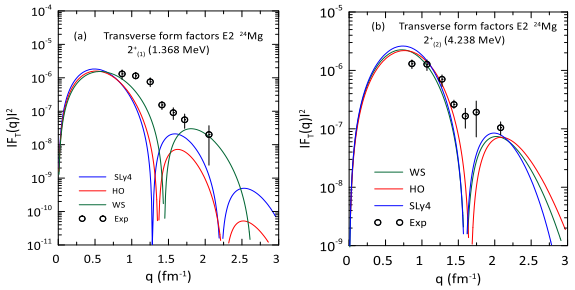

Figure 2. Transverse E2 form factor for $\mathbf{2^+_{(1)}}$ (1.368) MeV (a) and $\mathbf{2^+_{(2)}}$ (4.238) MeV (b) states, calculated using different single-particle potentials, in comparison with experimental data taken from Ref. [8].

Fig.3(a) illustrates the theoretical calculated M3 form factor for the purely magnetic $3^+_{(1)}$ transition using various single-particle potentials. While the calculated form factors underestimated the experimental data, they captured the overall pattern of the data. In order to improve the agreement, we examined the form factor's sensitivity to modifications in the two-body effective interactions (Fig.3(b)). It is clear that these interactions influence the characteristics of the inelastic calculations, and they improved the agreement with the experimental data, thus justifying reliance on the conclusions. The inelastic longitudinal C4 form factors for the $4^+_{(1)}$ and $4^+_{(1)}$ states are calculated using sdpf SM space illustrated in Figs. 4 and 5. It is apparent that the calculated results, utilizing various single-particle potentials, do not exhibit any alteration in the overall behavior of the form factor profiles.

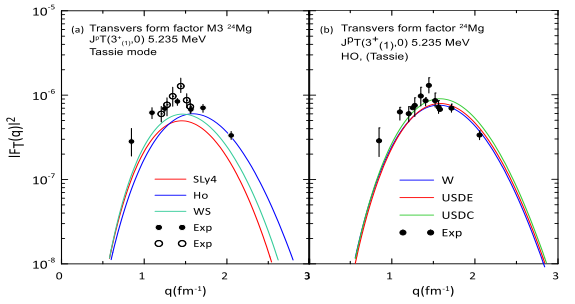

Figure 3. Transversal theoretical the first form factors 3^+, 5.235 MeV state (a) utilizing various single-particle potentials and (b) using different interaction compared with experiment results [8].

The $4^+_{(1)}$ form factor in Fig. 4(a) displays poor agreement with the experimental data, failing to accurately replicate the experimental shape. While the maximum of the calculated $4^+_{(1)}$ form factor aligns approximately with the measured value, the calculated shape deviates significantly from the experimental observation. In an effort to address the disparities with the experimental data in Fig. 4(b), sensitivity tests were conducted to assess the selected models.

However, it was observed that the general trends of the calculated C4 form factors inadequately mirrored the experimental data. The behavior of the nuclear form factor in this context may be influenced by the limitations of the chosen models in capturing the intricate dynamics of the nuclear system, leading to discrepancies between calculated results and experimental observations.

Further refinement of the theoretical framework and consideration of additional factors may be necessary to improve the agreement between calculated and experimental data.

Fig.5 (a) shows the longitudinal C4 form factor for the transition $4^+_{(2)}$. The calculated peak location and strength align pretty well with the data. When comparing it with the experimental data, it's noted that the form factor profile doesn't significantly change when altering the single particle potentials with each other or with the experimental data. However, with the SLy4 potential, the agreement with the experimental data gradually diverges as the momentum transfer increases. The comparison in Fig.4 (b) for the strong $4^+_{(2)}$ transition indicates that the calculated longitudinal E4 form factor curves underestimate the experimental data but effectively capture the general trend.

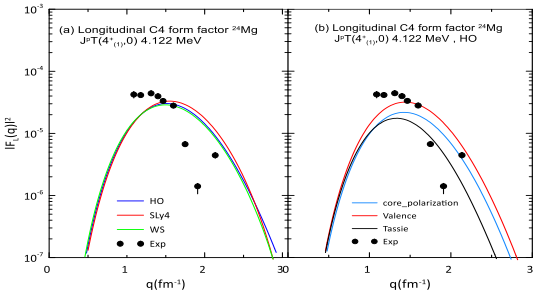

Figure 4. Theoretical for the longitudinal form factor 4.122 MeV state, the first 4^+ (a) making use of various single particle potentials and (b) using different model compared with experimental data [8].

It is noteworthy that the calculated curves for the $4^+_{(1)}$ and $4^+_{(2)}$ states share very similar shapes, while the data exhibits significant differences.

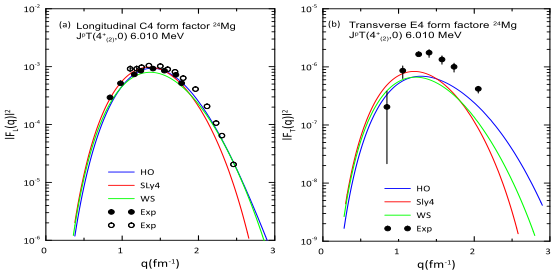

Figure 5. (a), A alternative single particle potential's the second 4^+, 6.010 MeV state's predicted longitudinal form factor and (b), Theoretical transvers form factor for second 4^+, 6.01MeV utilizing various single particle potentials in comparison with the experimental data [8].

This study only utilizes three single particle potentials, and there is a clear need for a better representation of collective features.

3.2. Negative Parity states

The need for studying the nuclear parity-changing transitions is apparent, as this would give one an appropriate understanding of the general principles of nuclear parity and the transition process between nuclear states. These transitions give details regarding the traits and facets of the inherent excitations in the nucleus, helping elucidate the strong and weak forces in the nucleus. Exploring parity-changing transitions offers rich insights into fundamental aspects of nuclear physics that help deepen our understanding of atomic nuclei's complex internal structures and behaviors at different excitation states. These transitions will be studied in ^{24}Mg, for which experimental data are available regarding their sensitivity of the electroexcitation form factors to changes in the single-particle potentials and nuclear models. The truncated large-scale shall model spsdpf with 1 ħω has been used to perform present calculations. This model space provides ample space for valence nucleons to create nuclear-excited states of different parity as needed. Numerous negative parity states have been identified. Based on the total angular momentum value, the results will be presented and discussed sequentially. Fig. 6 (a) shows the theoretical calculation of the inelastic total electro excitation form factors for the transition to the $1^-_{(1)}$ 7.555 MeV excited state, which indicates varying degrees of agreement and disagreement with the experimental data. The form factors calculated using the HO potential closely match the experimental data [7] within the relevant momentum transfer range. This indicates that the OH potential effectively represents the essential characteristics of the nuclear structure for this specific transition. While the WS and SHF potentials are useful in other scenarios, they may not capture the subtleties of this transition as effectively as the HO does. As shown in Fig. 6 (b), the good agreement of the HO potential with the experimental data also extends to the form factor in the second excited state $1^-_{(2)}$ 8.438 MeV. The calculation successfully reproduces the peak structure of the form factors. The deviation of the other potentials from experimental data could indicate that the model's complexity does not necessarily translate to improved accuracy for this transition.

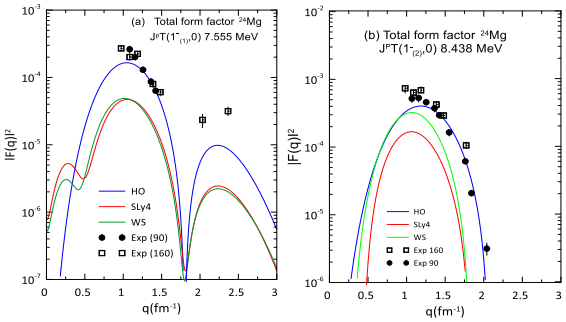

Figure 6. Total squared form factors for (a) $1^-_{(1)}$, 7.555 MeV state and (b) $1^-_{(2)}$, 8.438 MeV state $1^-_{(1)}$, using various single potentials in comparison with the experiment data [7].

The results shown in Fig. 7 indicate that the total electro excitation form factors for the transition to the $1^+_{(3)}$ 9.146 MeV state were calculated using different single-particle potentials incorporated with various models. Notably, the comparison with experimental data reveals that the SLy4 potential and the CP model produce the most favorable results compared to the experimental data. This suggests that the model can accurately describe the nuclear forces at work.

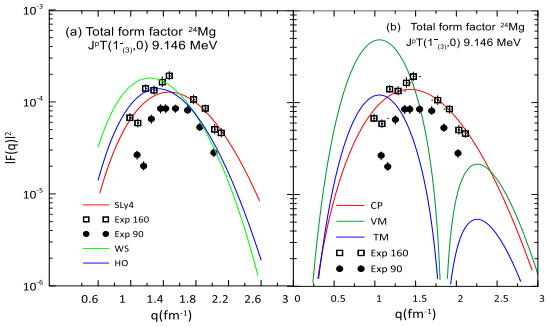

Figure 7. Total squared form factors for (a) $\mathbf{1}^-_{(3)}$, 9,146 MeV using various single potentials and (b) using different models in comparison with the experiment data [7].

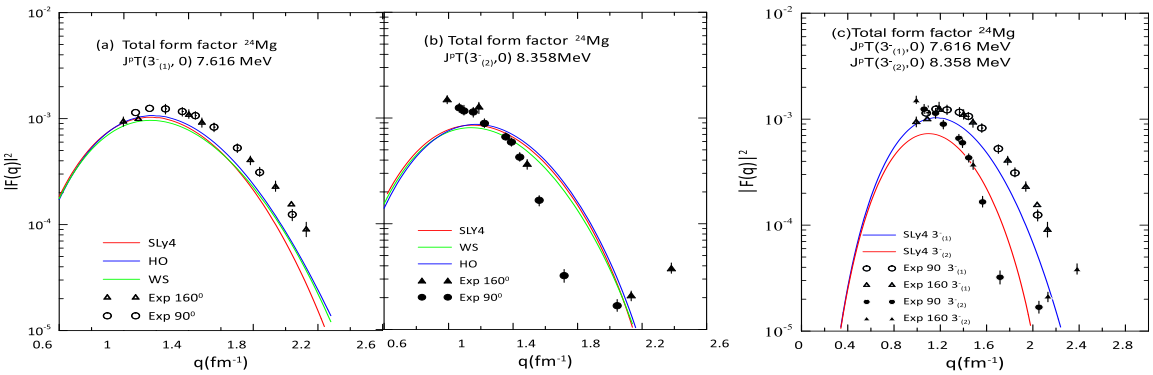

Figure 8. Total squared form factors the first $\mathbf{3}^-_{(1)}$ 7.616 MeV (a), and second $\mathbf{3}^-_{(2)}$ 8.358 MeV (b) states using different single-particle potentials with a comparison between them in (c) and with the experimental data. [7].

The present results highlight the importance of selecting the correct models and potentials to make accurate predictions for the transition to the negative parity state. The lowest two $3^-_{(1)}$, $3^-_{(2)}$ T=0 excited states in ^{24}Mg occur at excitation energies of 7.616 and 8.358 MeV. The total squared electro excitation form factors for these two states are calculated using different single-particle potentials and depicted in Fig. 8(a) and (b), compared with the available experimental data. It is obvious that the total form factors are insensitive to variation in the potential, even in parity-changing transition. The form factor profiles remain unchanged in the momentum transfer range of the experimental data, and the peak structure is reasonably reproduced.

Fig. 8 (c) depicts a comparison between $3^-_{(1)}$, $3^-_{(2)}$ inelastic total form factors (E3+C3), which demonstrates that the difference in shape grows gradually with increasing the momentum transfer. These states are different, with the $3^-_{(2)}$ state having a much larger transition radius than the $3^-_{(1)}$ state.

Fig. 9 displays the total electro excitation form factors for the first 5^- , 10.027 MeV and the first 6^- 17.600 MeV states, calculated using different single-particle potentials.

The form factor profiles demonstrate distinct shapes that mirror the underlying nuclear structure associated with these excited states. Specifically, for the 5^- state, it reveals a sharp peak, indicating a more localized nucleon distribution, which is characteristic of this excitation. This suggests that the 5^- state possesses a significant single-particle character, with nucleons being more tightly bound and exhibiting less collective motion.

In contrast, the form factor for the 6^- state exhibits a broader distribution, signaling a more complex configuration that may involve higher angular momentum contributions and increased collectivity among nucleons.

Upon comparing with experimental data, it is evident that there are varying degrees of agreement depending on the chosen single-particle potentials.

Notably, the results align more closely with the experimental data when employing the HO potentials, suggesting better capture of the nuclear structure's nuances and the dynamics of the excited states.

This alignment reinforces the validity of the theoretical models and underscores the significance of selecting suitable potentials in nuclear structure calculations.

Fig. 10 shows the transverse form factors for a specific nuclear state 2^- at 12.560 MeV using various single-particle potentials compared to experimental data [7]. This comparison evaluates how the theoretical models based on these potentials match the experimental data. It was found that the HO potential is in better agreement with the experimental data, indicating that, in this specific case, HO provides a closer match to experimental results for the transverse form factor of the 12.560 MeV state.

This suggests that HO may be more suitable or accurate for describing scattering processes at this energy level.

3.3 The excitation energies

In Fig.11 and Table 1, the energy levels for low-lying states and specific second and third sequences of positive and negative parity states in ^{24}Mg have been computed within the sd and truncated spsdpf SM spaces utilizing USDC and WBP two-body effective interactions.

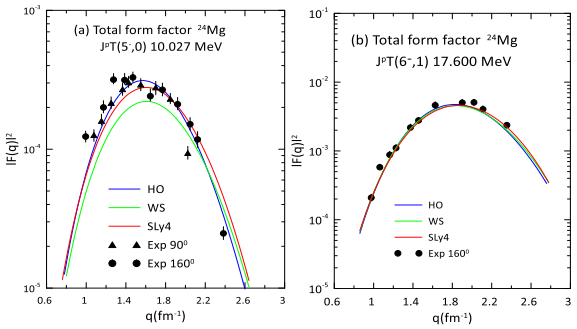

Figure 9. Total squared form factor for the first 5^-, 10.027 MeV state (a) and first 6^-, 17.600 MeV (b) using various single-particle potentials in comparison to the experimental data taken from Ref. [7].

The resulting spectrum is depicted through energy levels represented by red and blue lines denoting positive and negative parity states, respectively.

It is evident that most of the calculated excitation energies exhibit a reasonable agreement with experimental data [7], [8], except for a few levels corresponding to negative parity states. These observed discrepancies could be attributed to the truncation imposed on the spsdpd model space.

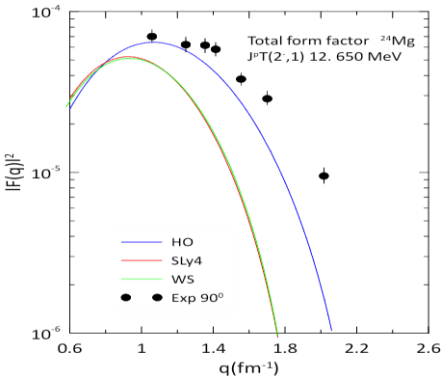

Figure 10. The transvers form factor for 2^- ,12.560 MeV state using various single-particle potentials in comparison to the experimental data taken from Ref. [7].

3.4. Quadrupole deformation density profile

The quadrupole deformation parameter β_2 provides direct insight into the intrinsic shape of the nucleus and its departure from spherical symmetry.

It is closely related to the mass quadrupole moment Q and the mean-square radius $\langle r^2\rangle^{1/2}$, and is calculated here using the HF+BCS framework with the SLy4 Skyrme interaction. The respective relation is:

$$\beta 2 = \sqrt{\frac{\pi}{5}}\,\frac{Q}{A\langle r^2\rangle^{1/2}} \qquad (14)$$

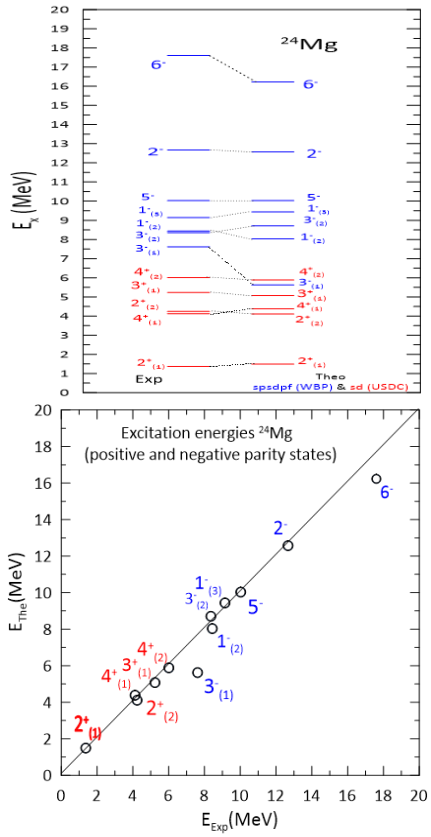

Figure 11. Energy levels for the negative parity states of ^{24}Mg nucleus compared with data taken from Ref. [7], [8] (left panel), with Comparison between the experimental and theoretical values (right panel).

where Q is the mass quadrupole moment and $<r^2>^{1/2}$ is the nucleus rms radius. Fig. 12 (left panel) shows the deformation energy surface of ^{24}Mg obtained from HF+BCS, now compared with a Nilsson-Strutinsky result.

Both models predict a prolate ground-state minimum at $\beta_2 \approx +0.5$, indicating a well-deformed axial configuration. A secondary oblate minimum is also visible near $\beta_2 \approx -0.2$, suggesting shape coexistence. However, the two curves differ quantitatively in both energy scale and surface curvature.

These differences can be attributed to the distinct physical assumptions behind the models. The HF+BCS method treats nucleons self-consistently in a deformed mean field and includes pairing correlations explicitly, yielding a more microscopically grounded energy surface.

In contrast, the Nilsson-Strutinsky model incorporates shell corrections and macroscopic deformation energies in a phenomenological way, which can sometimes exaggerate or smooth out energy valleys depending on parameter choices. As a result, the Nilsson-Strutinsky curve is generally smoother and shows a broader minimum, while the HF+BCS profile exhibits sharper features and a more localized minimum, reflective of the underlying shell structure and pairing dynamics.

Further support for a prolate-deformed ground state in ^{24}Mg is provided by fully microscopic calculations using the Anti-symmetrized Molecular Dynamics (AMD) model [10].

Table 1. Excitation energies for positive and negative parity states in ^{24}Mg.

J^π T	E_{Exp} (MeV)	E_{Theo} (MeV)
$1^-_{(2)}$ 0	8.437	8.031
$1^-_{(3)}$ 0	9.145	9.437
$2^-_{(3)}$ 1	12.650	12.572
$3^-_{(1)}$ 0	7.616	5.623
$3^-_{(2)}$ 0	8.357	8.705

These calculations predict a dominant intrinsic prolate configuration with deformation around $\beta_2 \approx 0.5$, consistent with the minima obtained from both the HF+BCS and Nilsson-Strutinsky approaches. While AMD does not yield a continuous deformation energy curve, its predictions offer an important complementary perspective that incorporates nucleon correlations and cluster-like configurations beyond the mean-field level. The right panel of Fig. 12 displays the proton, neutron, and total matter densities, along with the corresponding rms radii. The near-overlap of the proton and neutron distributions confirms the symmetry of the nucleus and the absence of a significant neutron skin. These density distributions are consistent with a well-bound, prolate deformed structure in ^{24}Mg. The positive value of β_2 implies prolate deformation, as also emphasized in Fig. 13, where the nucleus is shaped like an elongated oval. This configuration can be energetically preferred because nucleons are placed in higher energy levels, which is preferred for this kind of shape.

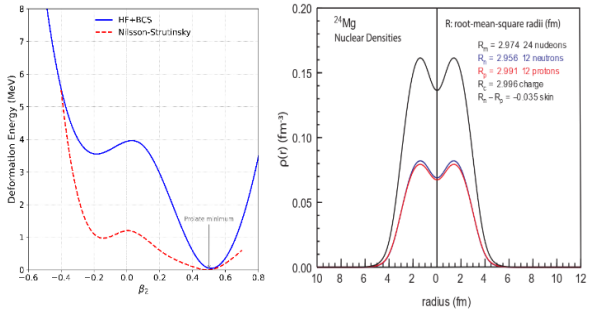

Figure 12. (Left) Deformation energy surface for ^{24}Mg from HF+BCS (SLy4) compared with Nilsson-Strutinsky results. (Right) Proton, neutron, and total radial density distributions and corresponding rms radii.

Prolate may increase the chances of nucleons occupying space far apart, hence reducing the chances of direct repulsion of protons, hence stabilizing the nucleus. Second minimum at $\beta_2 = -0.3$. This negative value depicts an oblate deformation in which the nucleus is flattened. The existence of this minimum suggests that there is an alternative configuration that is also energetically favorable. The oblate shape may arise from different nucleon configurations that minimize energy through pairing and spatial distribution, particularly in the presence of strong proton-proton repulsion. The fact of existence of two minima in the β_2 curve means that ^{24}Mg can have several stable or metastable structures. This is a characteristic of shape coexistence, which is the presence of more than one nuclear structure having almost the same energy. In the given context, the nature of energy shapes is related to the shell structure;

nucleons occupy specific energy levels, their interactions result in the competition of shapes.

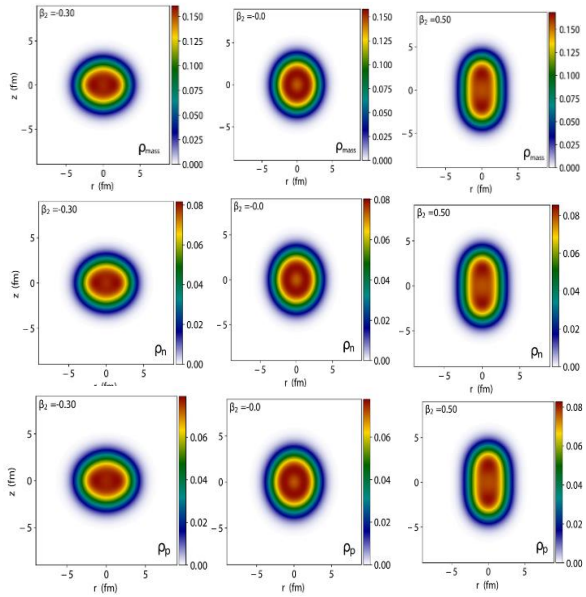

Figure 13. The two-dimensional plots of the mass, neutron, and proton density distributions at two separated minima of β2 values 0.5, -0.3 and 0 using HF+BCS.

Fig. 13 presents two-dimensional plots of mass, neutron, and proton density distributions at three different β_2 values, even in cases where the increase in employment is only slight, such as an extra 0. 5, -0. 3, and 0. This goes to show how the distribution of these densities is affected by the changes in the β2 values. At β_2 = 0. 5, the nucleus has to be more elongated or prolate and, therefore, has to have specifics in its distribution of mass, neutrons, and protons.

On the other hand, a β_2 has been estimated to be -0. 3 suggests a more oblate behavior, which would change the densities correspondingly. The case that $\beta_2 = 0$ is a spherical structure, which in a way, acts as the base system for the other two shapes.

4. Conclusions

From the results and discussions made in this work, the following conclusions can be drawn. By analyzing parity-changing transitions, one can gain information about nuclear characteristics and the processes that are connected to symmetry breaking. For both positive and negative parity states, the evaluated electromagnetic form factors are found to be sensitive to the choice of single-particle potential. Of all the potentials used, the HO potential provided the best mimic of the experimental data for the 1^- states, making it a good tool for studying nuclear structure for these specific transitions. However, as in the cases of M3 and C4, the theoretical predictions of form factors were lower than experimental ones. Despite potential imperfections, the overall trends and peaks indicate that theoretical models successfully capture the general qualitative behavior of nuclear excitation. The fact that the form factors depend on the changes in the two-body effective interactions brings the parameters into sharp focus as far as the description of the nuclear transitions is concerned. Changes to these interactions made the results converge better to the experimental values while underlining the fact that a certain amount of stiffness is essential for theoretical models. The behavior of β2 parameter as a function of energy indicates the shape coexistence in ^{24}Mg. It is proved that the nucleus can be in several more or less steady states with distinct β2 values. The nuclear density profile changes with deformations which are defined by the deformation parameter β2: prolate (elongated) and oblate (flattened). To emphasize here is the relationship between the nuclear shape and distribution density, which gives the fundamentals of the structural characteristic.

Authors Contribution

All the authors have participated sufficiently in the intellectual content, conception and design of this work or the analysis and interpretation of the data (when applicable), as well as the writing of the manuscript.

Availability of data and materials

The data that support the findings of this study are available from the corresponding author, upon reasonable request.

Conflict of interests

The author states that there is no conflict of interest.

References

[1] M. G. Mayer, "On closed shells in nuclei. II," *Phys. Rev.*, vol. 75, no. 12, pp. 1969–1970, 1949, doi: 10.1103/PhysRev.75.1969

[2] R. F. Casten and S. Moszkowski, "Nuclear Structure from a Simple Perspective," *Phys. Today*, vol. 44, no. 11, pp. 91–92, Nov. 1991, doi: 10.1063/1.2810324

[3] B. A. Brown, "The nuclear shell model towards the drip lines," *Prog. Part. Nucl. Phys.*, vol. 47, no. 2, pp. 517–599, Jan. 2001, doi: 10.1016/S0146-6410(01)00159-4

[4] R. A. Radhi and A. A. Alzubadi, "Study the Nuclear Form Factors of Low-Lying Excited States in ^{7}Li Nucleus Using the Shell Model with Skyrme Effective Interaction," *Few-Body Syst.*, vol. 60, no. 3, p. 57, Sep. 2019, doi: 10.1007/s00601-019-1524-x

[5] B. A. Brown and B. H. Wildenthal, "Status of the Nuclear Shell Model," *Annu. Rev. Nucl. Part. Sci.*, vol. 38, no. 1, pp. 29–66, Dec. 1988, doi: 10.1146/annurev.ns.38.120188.000333

[6] A. A. Alzubadi and R. S. Obaid, "Study of the nuclear deformation of some even–even isotopes using Hartree–Fock–Bogoliubov method (effect of the collective motion)," *Indian J. Phys.*, vol. 93, no. 1, pp. 75–92, 2019, doi: 10.1007/s12648-018-1269-2

[7] H. Zarek *et al.*, "Inelastic electron scattering to negative parity states of ^{24}Mg," *Phys. Rev. C*, vol. 29,

no. 5, pp. 1664–1671, May 1984, doi: 10.1103/PhysRevC.29.1664

[8] A. Hotta, R. S. Hicks, R. L. Huffman, G. A. Peterson, R. J. Peterson, and J. R. Shepard, "Transverse isoscalar excitations in ^{24}Mg by 180° electron scattering," *Phys. Rev. C*, vol. 36, no. 6, pp. 2212–2220, Dec. 1987, doi: 10.1103/PhysRevC.36.2212

[9] N. S. Manie and A. A. Alzubadi, "Electromagnetic multipole of positive and negative parity states in ^{24}Mg by elastic and inelastic electron scattering," *Iraqi J. Phys.*, vol. 17, no. 42, pp. 27–41, Aug. 2019, doi: 10.30723/ijp.v17i42.421

[10] Y. Kanada-En'yo and K. Ogata, "Microscopic coupled-channel calculation of proton and alpha inelastic scattering to the $\mathbf{4_1^+}$ and $\mathbf{4_2^+}$ states of ^{24}Mg ," *Phys. Rev. C*, vol. 103, no. 2, p. 024603, Feb. 2021, doi: 10.1103/PhysRevC.103.024603

[11] E. W. Lees, A. Johnston, S. W. Brain, C. S. Curran, W. A. Gillespie, and R. P. Singhal, "The study of the excited states of ^{26}Mg below 11 MeV by inelastic electron scattering," *J. Phys. A Math. Nucl. Gen.*, vol. 7, no. 8, pp. 936–974, May 1974, doi: 10.1088/0305-4470/7/8/005

[12] E. W. Lees, C. S. Curran, T. E. Drake, W. A. Gillespie, A. Johnston, and R. P. Singhal, "Inelastic electron scattering from ^{25}Mg," *J. Phys. G Nucl. Phys.*, vol. 2, no. 5, pp. 341–356, May 1976, doi: 10.1088/0305-4616/2/5/010

[13] T. T. S. Kuo and G. E. Brown, "Structure of finite nuclei and the free nucleon-nucleon interaction," *Nucl. Phys.*, vol. 85, no. 1, pp. 40–86, Sep. 1966, doi: 10.1016/0029-5582(66)90131-3

[14] T. T. S. Kuo, "State dependence of shell-model reaction matrix elements," *Nucl. Phys. A*, vol. 103, no. 1, pp. 71–96, Oct. 1967, doi: 10.1016/0375-9474(67)90790-7

[15] B. H. Wildenthal, E. C. Halbert, J. B. McGrory, and T. T. S. Kuo, "Calculations with a 1*s*, 0*d* Shell Model for *A* =34 −38 Nuclei," *Phys. Rev. C*, vol. 4, no. 4, pp. 1266–1314, Oct. 1971, doi: 10.1103/PhysRevC.4.1266

[16] E. K. Warburton and B. A. Brown, "Effective interactions for the 0 p 1 s 0 d nuclear shell-model space," *Phys. Rev. C*, vol. 46, no. 3, pp. 923–944, Sep. 1992, doi: 10.1103/PhysRevC.46.923

[17] A. A. Allami and A. A. Alzubadi, "Study of the Nuclear Structure of Some Exotic Nuclei Using Nonrelativistic and Relativistic Mean-Field Methods," Int. J. Mod. Phys. E, vol. 29, no. 12, p. 2050090, Dec. 2020, doi: 10.1142/S0218301320500901

[18] J. W. Negele and D. Vautherin, "Density-Matrix Expansion for an Effective Nuclear Hamiltonian," *Phys. Rev. C*, vol. 5, no. 5, pp. 1472–1493, May 1972, doi: 10.1103/PhysRevC.5.1472

[19] B. A. Brown *et al.*, "Shell-model analysis of high-resolution data for elastic and inelastic electron scattering on ^{19}F," *Phys. Rev. C*, vol. 32, no. 4, pp. 1127–1156, Oct. 1985, doi: 10.1103/PhysRevC.32.1127

[20] B. A. Brown and W. D. M. Rae, "The Shell-Model Code NuShellX@MSU," *Nucl. Data Sheets*, vol. 120, pp. 115–118, Jun. 2014, doi: 10.1016/j.nds.2014.07.022

[21] W. Rae, "NuShellX - Large Scale Shell Model Calculations on your PC.," *Garsington*, 2008. http://www.garsington.eclipse.co.uk/